2013

Parametric Average-Value Model of Rectifiers in Brushless Excitation Systems

Thaer Qunais
University of Kentucky, thaerissam@hotmail.com

STUDENT AGREEMENT:

I represent that my thesis or dissertation and abstract are my original work. Proper attribution has been given to all outside sources. I understand that I am solely responsible for obtaining any needed copyright permissions. I have obtained and attached hereto needed written permission statements(s) from the owner(s) of each third-party copyrighted matter to be included in my work, allowing electronic distribution (if such use is not permitted by the fair use doctrine).

I hereby grant to The University of Kentucky and its agents the non-exclusive license to archive and make accessible my work in whole or in part in all forms of media, now or hereafter known. I agree that the document mentioned above may be made available immediately for worldwide access unless a preapproved embargo applies.

I retain all other ownership rights to the copyright of my work. I also retain the right to use in future works (such as articles or books) all or part of my work. I understand that I am free to register the copyright to my work.

REVIEW, APPROVAL AND ACCEPTANCE

The document mentioned above has been reviewed and accepted by the student's advisor, on behalf of the advisory committee, and by the Director of Graduate Studies (DGS), on behalf of the program; we verify that this is the final, approved version of the student's dissertation including all changes required by the advisory committee. The undersigned agree to abide by the statements above.

Thaer Qunais, Student

Dr. Aaron M. Cramer, Major Professor

Dr. Cai-Cheng Lu, Director of Graduate Studies

PARAMETRIC AVERAGE-VALUE MODEL OF RECTIFIERS IN BRUSHLESS EXCITATION SYSTEMS

Thesis

A thesis submitted in the partial fulfillment of the
requirements for the degree of Masters of Science in Electrical Engineering
in the College of Engineering at the University of Kentucky.

By
Thaer Qunais
Lexington, Kentucky

Director: Dr. Aaron Cramer, Associate Professor
Department of Electrical and Computer Engineering
College of Engineering, University of Kentucky.

ABSTRACT OF THESIS

PARAMETRIC AVERAGE-VALUE MODEL OF RECTIFIERS IN BRUSHLESS EXCITATION SYSTEMS

An average-value model of a rotating rectifier circuit in a brushless excitation system is set forth, where a detailed simulation is required to extract the essential averaged-model parameters using numerical averaging. In the proposed approach, a synchronous machine model with saturation and cross saturation and an arbitrary rotor network representation that uses a voltage-behind-reactance representation for the field winding of the main machine is proposed. This allows the field winding to be represented as branches in a circuit solver, permitting straightforward simulation with connected circuitry. Also a brushless exciter model is introduced to be compatible with the averaged-model, where the exciter armature windings are represented using a voltage-behind-reactance formulation. The resulting average-value model is verified in time domain against detailed simulation, and its validity is demonstrated in all rectifier modes of operation.

Keywords: Average-value model (AVM), Electric machines, modeling, synchronous generator excitation, synchronous machines.

Thaer Qunais

12/18/13

PARAMETRIC AVERAGE-VALUE MODEL OF RECTIFIERS IN BRUSHLESS EXCITATION SYSTEMS

By
Thaer Qunais

Director of Thesis: Dr. Aaron Cramer
Director of Graduate Studies: Dr. Cai-Cheng Lu
Date: 12/18/13

Dedication

To my parents, Issam Qunais and Yusra Elayan, for their love, endless support and encouragement.
To my late grandmother Lateefa Farhan, her words of inspiration and encouragement in pursuit of excellence, still linger on.
To my dear aunt Taghreed Qunais, her support and constant love have sustained me throughout my childhood.
To Prof. Yahya Farhan, for his guidance and for instilling the importance of hard work and higher education.
To my sincere friend Hassan Al-Omari, thanks for making me believe that everything is going to be okay.
I will always appreciate all you have done.

Acknowledgements

I would like to express the deepest appreciation to my committee chair Dr. Aaron Cramer, who has shown the attitude and the substance of a genius: he continually and persuasively conveyed a spirit of adventure in regard to research, and an excitement in regard to teaching. Without his supervision and constant help this thesis would not have been possible.

I wish to thank my committee members who were more than generous with their expertise and precious time. Thank you Dr. Yuan Liao, and Dr. Zhi Chen for agreeing to serve on my committee.

Contents

List of Tables

List of Figures

Chapter 1

Introduction

Mathematical models use the language of mathematics to describe, understand and evaluate systems effectively. Mathematical models are used in the natural sciences and engineering disciplines. A mathematical model usually describes a system by a set of variables and a set of equations that establish relationships between the variables.

The synchronous machine as an ac generator is the main electric power generating source throughout the world. Diode rectifiers connected to synchronous machines are used in a wide variety of applications. For example, generator-rectifier systems are used in shipboard and aircraft dc power distribution systems (e.g., [1] and [2], respectively), high power dc supplies [3], and excitation systems of large electric generators [4].

A brushless excitation system consists of an ac exciter and a rotating rectifier mounted on the same shaft as the main machine field circuit. Brushless excitation of synchronous machines offers the advantages of improved reliability, improved maintenance, and improved performance [5], since it eliminates the need for mechanical parts like slip rings and brushes.

A detailed simulation which includes all synchronous machine dynamics, dc link dynamics, and semiconductor switching states yields very accurate results; however, detailed simulations for systems including rectifiers are computationally intensive. Detailed computer simulation of switching systems is usually useful when diode failures [6] are of interest, since it provides design evaluation and helps identify potential design problems before serious hardware failure occurs or when the effect of higher order harmonics is significant. However, the exact switching behavior predicted by detailed models are not of interest in many applications. Therefore, to reduce modeling complexity of such systems and improve its computational efficiency an average value model of the rectifier should be derived wherein the rectification process is represented on an average basis.

In this work, a numerical averaging of the rotating rectifier in a brushless excitation system is presented. In the proposed averaged model, the parameters defining the relationship between the averaged dc variables and the exciter variables transformed to the stationary reference frame are extracted from a detailed simulation, and vary depending on the loading conditions that are specified in terms of a dynamic impedance.
A brushless exciter model is set forth to be compatible with the averaged model, where the subtransient open-circuit voltages are available to calculate the dynamic impedance. The brushless exciter′s equations are rewritten in such a way as to allow the actual armature windings to be represented using a voltage-behind-reactance (VBR) formulation.
Although implementing the averaged model requires running the detailed simulation in a wide range of loading conditions, once this is done, the resulting model is continuous and valid for time-domain studies.
The main machine model is proposed by formulating a voltage-behind–reactance representation for the field winding, which can be directly connected to the rotating rectifier.

Chapter 2

Background and Literature Review

2.1 Synchronous Machines

The synchronous machine is an ac machine that is most often used to convert mechanical energy to ac electrical energy. The two main parts of a synchronous machine are the stationary part called the stator and the rotating part called the rotor. The rotor can be cylindrical, or it can have pole faces projecting out from its surface. If the rotor is cylindrical, the machine is said to have nonsalient poles; if the rotor has pole faces projecting out from it, the machine is said to have salient poles as shown in Figure 2.1 .

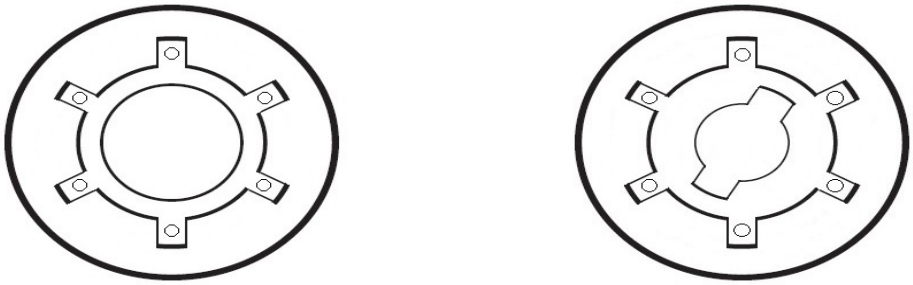

Figure 2.1: Left: An ac machine with a nonsalient-pole rotor. Right: An ac machine with a salient-pole rotor.

Synchronous machines are equipped with multiple windings. The field winding is the winding that produces the main magnetic field in the machine when it is energized. Armature windings are the windings where the main currents are induced. Short circuited damper windings are also present to improve the dynamic response of the machine to power system transients and improve stability, but these windings do not affect the steady-state performance of the machine. For typical synchronous machines, the field and damper windings are mounted on the rotor. The armature windings are distributed in longitudinal slots in the stator; thus, the terms stator windings and armature windings are the same [7]. It is typically assumed that all of the windings are distributed such that they produce a sinusoidally distributed air gap flux.

In a synchronous generator, a dc current is supplied to the field winding, and the rotor shaft is driven by a prime mover, which is usually a steam or hydraulic turbine. This produces a rotating magnetic field. This rotating magnetic field induces a three-phase set of voltages across the stator windings of the generator.

In larger power systems, the power output of the generator is controlled by adjusting the power output of the prime mover. The reactive power is controlled by adjusting the voltage applied to the field winding or the machine′s excitation. In smaller systems, the excitation is used to control the

magnitude of the generator′s output voltage. A special arrangement is required to excite the machine because the field winding is rotating. It is possible to supply dc power to the field winding by means of slip rings and brushes, but this arrangement creates a few problems when it is used. The brushes must be checked for wear regularly since mechanical contact occurs between the rotor and the stator; thus they increase the amount of maintenance required on the machine. In addition, on machines with large field currents the brush voltage drop can cause significant power loss. Alternatively a brushless exciter is often used to supply the dc field current to the machine. An exciter is a small ac generator with its field circuit mounted on the stator and its armature circuit mounted on the rotor shaft [8]. By exciting the stationary field winding of the exciter, ac voltage is produced in the rotating armature windings. A rotating rectifier converts this to dc voltage which is used to excite the field winding of the main machine.
For synchronous machines, there are several models that may be used to predict their steady-state or dynamic behavior. The majority of the models are expressed through Park′s transformation [9], in terms of variables of fictitious windings in the rotor frame of reference.
Park′s transformation is a well-known technique that is often used in the analysis of electric machines, where the variables (voltages, currents, and flux linkages) of the stationary abc phases in a synchronous machine are transferred to three equivalent $qd0$ phases rotating at the same speed of the rotor, this change of variables is often used to reduce the complexity of the machine differential equations.
Among the advantages of using this transformation are that (1) the resulting equations are independent of rotor position (time-invariant) and do not have time-varying inductances from the voltage equations of the synchronous machine that occur due to electric circuits in relative motion and electric circuits with varying magnetic reluctance and (2) the state variables (currents or flux linkages) are constant in the steady state. This simplifies both the steady-state and dynamic analysis of the machine.

2.2 Rectification

Rectification is the process of converting an alternating (ac) voltage into one that is limited to one polarity. Rectification can be classified as half-wave or full-wave, with half-wave being the simpler and full-wave being more efficient [10]. So a rectifier circuit is a circuit that converts ac power to dc power.
The circuit of a three-phase full wave rectifier is shown in Figure 2.2, the diodes are numbered in the order of conduction sequences. The conduction sequence for diodes is 12, 23, 34, 45, 56, and 61.

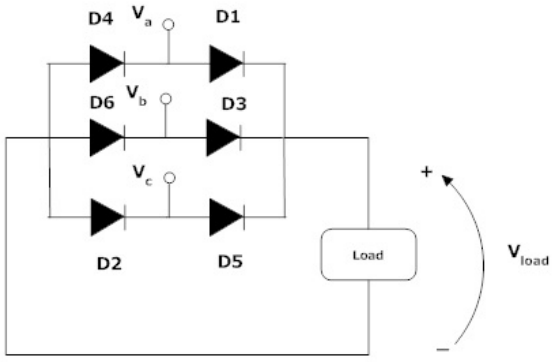

Figure 2.2: A three-phase full-wave rectifier circuit.

The brushless exciter in this study will be connected to a three-phase full wave diode rectifier.

Commutation

Ideally in rectifier circuits the diode currents transfer (commutate) from one diode to another instantaneously as shown in Figure 2.3 . However this cannot happen when the AC source has some inductance since the change of current through any inductance must take some time. The commutation process forces more than a pair of diodes in a bridge rectifier to conduct simultaneously.
Refer to Figure 2.2, and take into account the ac source inductance. At the time that V_b is about to become larger than V_a, due to source inductance in phase a, the current in D1 cannot fall to zero immediately. Similarly, due to the inductance in phase b, the current in D3 cannot increase immediately to its full value. The result is that both diodes conduct for a certain period as shown in Figure 2.4 , which is called the overlap (or commutation) angle [11].

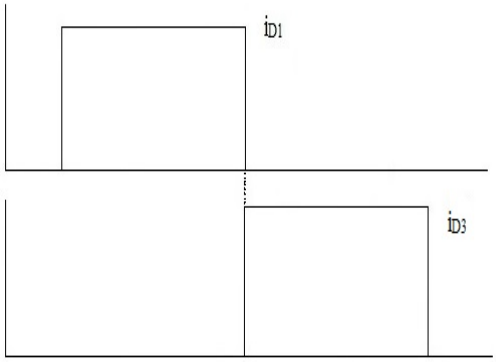

Figure 2.3: Diodes current in ideal rectifier.

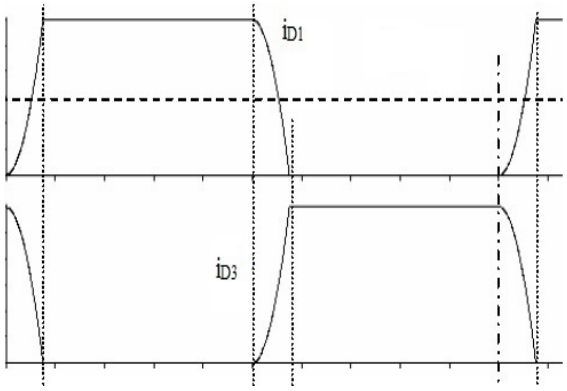

Figure 2.4: Current commutation.

Modes of operation

The average value model of the rectifier circuit introduced in this work is valid for all rectifier operating modes [12].

First mode of operation

The first mode may be divided into two distinct intervals; the commutation interval and the conduction interval. The first interval extends from $\pi/6$ at the start of commutation from D5 to D1,

to $\pi/6 + u$ at the end of commutation, where u denotes the commutation angle which lasts for less than $\pi/3$ in this mode of operation, in this interval three diodes are conducting (1, 5 and 6).
During the second interval from $\pi/6 + u$ to $\pi/2$, when another commutation interval starts, only D1 and D6 are conducting.

Second mode of operation

In this mode commutation becomes continuous and three diodes are always conducting. The commutation angle u remains constant at $\pi/3$, but a forced delay in commutation is introduced by an angle α which varies between 0 to $\pi/6$.

Third mode of operation

In this mode the delay angle α remains fixed at $\pi/6$, and the commutation angle u varies between $\pi/3$ to $2\pi/3$.
This mode may be divided into two intervals, the first interval extends from $\pi/2$ to $u+\pi/6$, four diodes are conducting (1, 2, 5 and 6); two commutations are taking place simultaneously; and a temporary three-phase short circuit is applied to the rectifier.
At $u+\pi/6$ the commutation from D5 to D1 finishes. During $u+\pi/6$ to $5\pi/6$, there are three diodes (1, 2 and 6) conducting and a line-to-line short circuit is imposed on the rectifier.

2.3 Literature Review

Synchronous machine models

Numerous synchronous machine models have been proposed so far to accurately represent generators for analysis by modern computer simulation software, such as Matlab/Simulink [13].
In [14], [15] high-order synchronous machine models are introduced, where the rotor circuit contains multiple damper windings in each axis. A standstill frequency response (SSFR) test [16] data is used to identify the synchronous machine models. Sinusoidal currents of small magnitude and different frequencies are applied to the machine at standstill. Based on the reactions of the machine the desired frequency responses of the direct and quadrature axis are established.
Unlike the standard models used in [14], [15], where the field and damper circuits are coupled, a new generator model is set forth in [17], such that the field and damper circuits are decoupled, the leakage fields as well as the eddy currents of the two circuits are independent from each other and modeled by two separate, branching "ladder networks" attached to the network common to both, the RL ladder network parameters are identified by combining the standstill frequency response measurements with the results of the standardized three phase no-load short-circuit test.
Later studies [18] show that no unique RL ladder network representation exists for models containing more than one damper winding. In [18] the starting-point is the Z -matrix (impedance matrix) of the d-axis network as it describes all two-port information in a unique way, where it was shown that different sets of RL circuit elements corresponding to the same Z –matrix can be found, and only a limited number of parameters (the main inductance, the stator leakage inductance, and the stator and rotor resistances) can be determined in a unique way from two-port information.
Some of the models [19], [20] require performing standard three-phase short-circuit test for determining the reactances and resistances of the equivalent circuit, the test is carried out with no load, the machine is rotating at rated speed and excited by a constant voltage applied to the field winding, the three phases are short-circuited simultaneously. The transient and subtransient time constants and reactances of the direct axis can be extracted from these tests.
The fundamental machine parameters are then expressed in terms of the measured time constants. However, these models avoid the effect of magnetic saturation.
A recent work proposed a synchronous machine model, where the rotor is represented by completely arbitrary linear circuits, a two-port network for the d-axis, and a single branch for the q-axis [21],

the transfer functions of these linear circuits can be obtained using standstill frequency response tests [22], which can then be realized to get the state matrices and solve for the state variables, therefore such a model avoids the time-consuming process of identification of the equivalent circuit parameters.
The magnetic saturation (and cross saturation) effects are considered in both axes, the analysis takes place in the rotor reference frame, and the proposed model is implemented as a voltage-in, current-out model, inputs are the stator and field winding voltages, while outputs are the stator and field winding currents.
This approach has been adopted from a previous induction machine model [23]. It offers the advantage that once the transfer functions of the rotor linear circuits are determined, they may be directly used in the model, on the other hand, it was expressed in qd-axes, voltage-in, current-out form, thus creating interface mismatch problems in both the stator windings of the machine and the field winding when connected with surrounding circuits.
Later studies on synchronous machine/converter system analysis reformulated the machine's equations in a VBR form.
A VBR model can be used to separate the rotor and stator dynamics, such that the rotor is represented by arbitrary linear networks, and the stator windings are represented by inductive branches (with mutual resistance and inductance), each branch also contains a voltage source that is controlled by the internal system states, thus it is called a stator VBR (SVBR) model [24].
The SVBR model allows the stator branches to be directly connected to other circuit elements (e.g., a rectifier). However, an important limitation remains in that SVBR formulation. The model still uses a voltage-in, current-out form for the field winding of the machine. This causes an interface problem when simulating a field winding being driven by a rotating rectifier in a brushless excitation system in a manner that is both accurate and numerically efficient.
In [25] a reformulation of the SVBR model [24] was developed that represents both the field winding and the stator windings as voltage sources behind time-varying impedances (which may include self and mutual coupling terms).
This developed Stator and field VBR (SFVBR) model is mathematically equivalent to the previous models, but it is formulated in a way that it is more helpful in simulation of systems where the field winding of the machine is connected to external circuits (e.g., a rotating rectifier in a brushless excitation system).
In this way, the SFVBR machine model avoids interface mismatch problem in simulations involving rectifier loads at the stator terminals and/or rectifier sources at the field winding.
In this work a brushless excitation system is considred, and the main machine/rectifier configuration in the field winding side only is of interest, thus an FVBR (field VBR) will be developed for the main machine, this allows the actual field winding to be represented by an inductive branch, which can then be connected to the rotating rectifier in the brushless excitation system.

Rectifier average-value models

Initial efforts toward the derivation of accurate average-value models (AVMs) for synchronous machine-rectifier systems started in the late 1960s. In [26] a suitable functional representation of the rectifier was derived and employed in a later work [27], that representation of the rectifier established a relationship between the ac source voltages and currents after being transformed into a frame of reference fixed in the rotor of the synchronous machine and the average dc variables of the rectifier, where a constant reactance behind a voltage source was used as a generator model, in this classical model the d-axis subtransient reactance was used as commutating reactance which is the series reactance of the ac source.
Reduced-order average-value model of synchronous machine-rectifier system was set forth in [28], [29]. Voltage-behind-reactance model was used to represent the synchronous machine, this model showed more accurate results in the steady-state compared to the classical model, since it assumed the equivalent commutating reactance as a function of both the q- and d-axes subtransient reactances which are generally different. However it neglects the stator dynamics of the synchronous machine

and therefore does not accurately predict the output impedance at higher frequencies.
An average-value model which is identical to the model set forth in [28] in the steady-state, but includes the effect of stator dynamics which are combined with the dc link dynamics was set forth in [30]. The model proposed was shown to be very accurate in predicting both the transient and steady state characteristics of the synchronous machine-rectifier system, and it was also shown to be much more accurate than classical models in which the stator dynamics are neglected. This work was extended to introduce an average value model of a synchronous machine/converter in which there is no dc link filter inductor in [31], the converter acts like a voltage source since the dc-link source is a voltage rather than a current, a reduced order synchronous machine model is also used in this model, simply the dc- link capacitor dynamics are considered in the dc-link model.
While in the previous cases ([26]- [30]), the AVM was developed analytically based on conduction and commutation intervals, and therefore was valid only for that operating mode, the study in [32], [33] assumes an approach similar to the one used in [27] and applies it to a three-phase synchronous generator with a diode-rectified output, a detailed simulation was used to extract the parameters of the rectifier AVM, to establish a relationship between the rectifier averaged dc output voltage and the main machine currents and voltages expressed in the *qd* form. These extracted parameters are independent of the loading conditions.
The approach introduced in [34] is an extension to the work of [33], where a detailed simulation was also required to obtain the AVM parameters which are essentially nonlinear algebraic functions using numerical averaging. However, unlike [33], the AVM parameters in this work vary depending on the loading conditions, and therefore it was shown to be more accurate in different rectifier modes.
This work follows the approach introduced in [34], an average value model of the rotationg rectifier feeding the main machine field circuit is derived, in the resulting AVM, a relationship between the rectifier averaged dc variables and the brushless exciter currents and voltages expressed in the *qd* form is established, this relationship is defined by some parameters that are extracted from the detailed simulation, and vary depending on the loading conditions.
A *qd* VBR model of the brushless exciter is also derived to be used with the proposed AVM.

Chapter 3

Field Voltage-Behind-Reactance Model

A voltage-behind-reactance formulation of a synchronous machine model which incorporates saturation and cross saturation, and uses an arbitrary rotor network representation is proposed, in particular, the model is simulated with a rectifier source applied to the field winding.
Since a brushless excitation system is of interest in this study, a VBR model is developed for the field winding only, the proposed FVBR model allows the field winding to be represented by an inductive branch in a circuit solver, permitting straightforward simulation when connected with a rectifier source in a brushless excitation system.

3.1 Notation

Matrices and vectors are boldfaced. Stator phase variables can be represented in vector form as $\mathbf{f}_{abcs} = [f_{as}\ f_{bs}\ f_{cs}]^{\mathrm{T}}$. The symbol f can represent voltage (v), current (i), or flux linkage (λ). Such vector quantities can be transformed into the rotor reference frame using

$$\mathbf{f}_{qd0s} = \mathbf{K}_s(\theta_r)\mathbf{f}_{abcs} \tag{3.1}$$

where the transformation matrix [9] is given by

$$\mathbf{K}_s(\theta_r) = \frac{2}{3}\begin{bmatrix} \cos\theta_r & \cos(\theta_r - \frac{2\pi}{3}) & \cos(\theta_r + \frac{2\pi}{3}) \\ \sin\theta_r & \sin(\theta_r - \frac{2\pi}{3}) & \sin(\theta_r + \frac{2\pi}{3}) \\ \frac{1}{2} & \frac{1}{2} & \frac{1}{2} \end{bmatrix}. \tag{3.2}$$

The electrical angular position of the rotor is given by

$$\theta_r = \frac{P}{2}\theta_{rm} \tag{3.3}$$

where P is the number of magnetic poles in the machine and θ_{rm} is the mechanical angular position of the rotor. Similarly, the electrical angular velocity of the rotor is given by

$$\omega_r = \frac{P}{2}\omega_{rm} \tag{3.4}$$

where ω_{rm} is the mechanical angular velocity of the rotor. The components of $\mathbf{f}_{qd0s} = [f_{qs}\ f_{ds}\ f_{0s}]^{\mathrm{T}}$ are the q- and d-axis components and the zero component of the quantity, respectively. When the zero component is omitted, $\mathbf{f}_{qds} = [f_{qs}\ f_{ds}]^{\mathrm{T}}$. The notation $\mathbf{f}_{dqs} = [f_{ds}\ -f_{qs}\ 0]^{\mathrm{T}}$ is used for speed voltage terms. Throughout, the operator p denotes differentiation with respect to time.

3.2 Original qd model

The development of the proposed model largely follows the development presented in [25]
The stator voltages are given by

$$\mathbf{v}_{abcs} = r_s \mathbf{i}_{abcs} + p\boldsymbol{\lambda}_{abcs} \tag{3.5}$$

where r_s is the stator resistance. Transforming (3.5) into the rotor reference frame yields

$$\mathbf{v}_{qd0s} = r_s \mathbf{i}_{qd0s} + \omega_r \boldsymbol{\lambda}_{dqs} + p\boldsymbol{\lambda}_{qd0s} \tag{3.6}$$

The stator flux linkages can be divided into a leakage term and a magnetizing term:

$$\boldsymbol{\lambda}_{qds} = L_{ls}\mathbf{i}_{qds} + \boldsymbol{\lambda}_{mqd} \tag{3.7}$$

where L_{ls} is the stator leakage inductance and $\boldsymbol{\lambda}_{mqd}$ are the magnetizing flux linkages. Solving (3.6) for $p\boldsymbol{\lambda}_{qds}$, equating with the time derivative of (3.7), and solving for $p\mathbf{i}_{qds}$ yields

$$p\mathbf{i}_{qds} = \frac{\mathbf{v}_{qds} - r_s\mathbf{i}_{qds} - \omega_r\boldsymbol{\lambda}_{dqs} - p\boldsymbol{\lambda}_{mqd}}{L_{ls}}. \tag{3.8}$$

The magnetizing currents are related to the magnetizing flux linkages by

$$i_{mq} = \Gamma_{mq}(\hat{\lambda}_m)\lambda_{mq} \tag{3.9}$$

$$i_{md} = \Gamma_{md}(\hat{\lambda}_m)\lambda_{md} \tag{3.10}$$

where $\Gamma_{mq}(\cdot)$ and $\Gamma_{md}(\cdot)$ are inverse inductance functions related to the representation of saturation [35] and

$$\hat{\lambda}_m = \sqrt{\lambda_{md}^2 + \alpha\lambda_{mq}^2} \tag{3.11}$$

where α is a saliency-dependent parameter. The relationship between the time derivatives of the magnetizing currents and of the magnetizing flux linkages is given by

$$p\mathbf{i}_{mqd} = \boldsymbol{\Gamma}_{mi}(\boldsymbol{\lambda}_{mqd})p\boldsymbol{\lambda}_{mqd} \tag{3.12}$$

where the incremental inverse inductance matrix is given by

$$\boldsymbol{\Gamma}_{mi}(\boldsymbol{\lambda}_{mqd}) = \begin{bmatrix} \frac{d\Gamma_{mq}(\hat{\lambda}_m)}{d\hat{\lambda}_m}\frac{\alpha\lambda_{mq}^2}{\hat{\lambda}_m} + \Gamma_{mq}(\hat{\lambda}_m), & \frac{d\Gamma_{mq}(\hat{\lambda}_m)}{d\hat{\lambda}_m}\frac{\lambda_{mq}\lambda_{md}}{\hat{\lambda}_m} \\ \frac{d\Gamma_{md}(\hat{\lambda}_m)}{d\hat{\lambda}_m}\frac{\alpha\lambda_{mq}\lambda_{md}}{\hat{\lambda}_m}, & \frac{d\Gamma_{md}(\hat{\lambda}_m)}{d\hat{\lambda}_m}\frac{\lambda_{md}^2}{\hat{\lambda}_m} + \Gamma_{md}(\hat{\lambda}_m) \end{bmatrix}. \tag{3.13}$$

$\boldsymbol{\Gamma}_{mi}(\cdot)$ is required to be symmetric since lossless coupling field is assumed .
The rotor circuit is represented in both the q- and d-axes by an arbitrary linear network. In particular, the d-axis is described by

$$p\mathbf{z}_d = \mathbf{A}_d\mathbf{z}_d + [\mathbf{A}_d\mathbf{b}_{d1}\ \mathbf{b}_{d2}]\begin{bmatrix} \lambda_{md} \\ v_{fdr} \end{bmatrix} \tag{3.14}$$

$$\begin{bmatrix} i_{dr} \\ i_{fdr} \end{bmatrix} = \begin{bmatrix} \mathbf{c}_{d1}^{\mathrm{T}} \\ \mathbf{c}_{d2}^{\mathrm{T}} \end{bmatrix}(\mathbf{z}_d + \mathbf{b}_{d1}\lambda_{md}) \tag{3.15}$$

and the q-axis is described by

$$p\mathbf{z}_q = \mathbf{A}_q\mathbf{z}_q + \mathbf{A}_q\mathbf{b}_q\lambda_{mq} \tag{3.16}$$

$$i_{qr} = \mathbf{c}_q^{\mathrm{T}}(\mathbf{z}_q + \mathbf{b}_q\lambda_{mq}). \tag{3.17}$$

The matrices $\mathbf{A}_d$, $\mathbf{B}_d = [\mathbf{b}_{d1}\ \mathbf{b}_{d2}]$, and $\mathbf{C}_d = [\mathbf{c}_{d1}\ \mathbf{c}_{d2}]^{\mathrm{T}}$ are a minimal realization of the d-axis rotor network transfer function, denoted by $\mathbf{Y}_d(s)$, and the components of $\mathbf{z}_d$ are state variables related

to this realization. Likewise, the matrix $\mathbf{A}_q$ and the vectors $\mathbf{b}_q$ and $\mathbf{c}_q$ are a minimal realization of the q-axis rotor network transfer function, denoted $Y_q(s)$, and the components of $\mathbf{z}_q$ are related state variables.
Taking the time derivative of the rotor and field currents and substituting (3.14) and (3.16) gives

$$pi_{dr} = \mathbf{c}_{d1}^{\mathrm{T}}(\mathbf{A}_d\mathbf{z}_d + \mathbf{A}_d\mathbf{b}_{d1}\lambda_{md} + \mathbf{b}_{d1}p\lambda_{md} + \mathbf{b}_{d2}v_{fdr}) \tag{3.18}$$

$$pi_{fdr} = \mathbf{c}_{d2}^{\mathrm{T}}(\mathbf{A}_d\mathbf{z}_d + \mathbf{A}_d\mathbf{b}_{d1}\lambda_{md} + \mathbf{b}_{d1}p\lambda_{md} + \mathbf{b}_{d2}v_{fdr}) \tag{3.19}$$

$$pi_{qr} = \mathbf{c}_q^{\mathrm{T}}(\mathbf{A}_q\mathbf{z}_q + \mathbf{A}_q\mathbf{b}_q\lambda_{mq} + \mathbf{b}_q p\lambda_{mq}). \tag{3.20}$$

Solving (3.19) for $\mathbf{v}_{fdr}$ yields

$$v_{fdr} = \frac{pi_{fdr} - \mathbf{c}_{d2}^{\mathrm{T}}(\mathbf{A}_d\mathbf{z}_d + \mathbf{A}_d\mathbf{b}_{d1}\lambda_{md} + \mathbf{b}_{d1}p\lambda_{md})}{\mathbf{c}_{d2}^{\mathrm{T}}\mathbf{b}_{d2}}. \tag{3.21}$$

Kirchhoff's current law relates the stator, magnetizing, and rotor currents:

$$\mathbf{i}_{qds} = \mathbf{i}_{mqd} + \mathbf{i}_{qdr}. \tag{3.22}$$

3.3 Proposed FVBR Model Formulation

It is possible to partition $\mathbf{z}_d$ such that

$$\mathbf{z}_d = \begin{bmatrix} z_{d1} \\ \bar{\mathbf{z}}_d \end{bmatrix}. \tag{3.23}$$

Such a partition requires that the the dimension of $\mathbf{z}_d$ be greater than or equal to 1. Solving (3.15) for $\mathbf{z}_{d1}$ yields

$$\mathbf{z}_{d1} = \frac{1}{(\mathbf{c}_{d2})_1}(i_{fdr} - \bar{\mathbf{c}}_{d2}^{\mathrm{T}}\bar{\mathbf{z}}_d - \mathbf{c}_{d2}^{\mathrm{T}}\mathbf{b}_{d1}\lambda_{md}) \tag{3.24}$$

where $(\mathbf{x})_i$ represents the ith element of vector $\mathbf{x}$ and $\bar{\mathbf{c}}$ represents the vector $\mathbf{c}$ with the first element removed. It is possible to partition $\mathbf{A}_d$ such that

$$\mathbf{A}_d = \begin{bmatrix} \mathbf{a}_{d1} & \bar{\mathbf{A}}_d \end{bmatrix}. \tag{3.25}$$

It is assumed that $(\mathbf{c}_{d1})_1 = 0$, such that the d-axis rotor current can be expressed as

$$i_{dr} = \bar{\mathbf{c}}_{d1}^{\mathrm{T}}\bar{\mathbf{z}}_d + \mathbf{c}_{d1}^{\mathrm{T}}\mathbf{b}_{d1}\lambda_{md} \tag{3.26}$$

and the stator currents can be expressed in terms of the state variables of the model by (3.22). Substituting (3.21) into (3.18) gives

$$\begin{aligned} pi_{dr} = \mathbf{c}_{d1}^{\mathrm{T}}\Bigg[&\mathbf{A}_d\mathbf{z}_d + \mathbf{A}_d\mathbf{b}_{d1}\lambda_{md} + \mathbf{b}_{d1}p\lambda_{md} \\ &+ \mathbf{b}_{d2}\frac{pi_{fdr} - \mathbf{c}_{d2}^{\mathrm{T}}(\mathbf{A}_d\mathbf{z}_d + \mathbf{A}_d\mathbf{b}_{d1}\lambda_{md} + \mathbf{b}_{d1}p\lambda_{md})}{\mathbf{c}_{d2}^{\mathrm{T}}\mathbf{b}_{d2}}\Bigg] \\ = \mathbf{c}_\chi^{\mathrm{T}}&\mathbf{A}_d(\mathbf{z}_d + \mathbf{b}_{d1}\lambda_{md}) + \mathbf{c}_\chi^{\mathrm{T}}\mathbf{b}_{d1}p\lambda_{md} + \chi pi_{fdr} \end{aligned} \tag{3.27}$$

where

$$\chi = \mathbf{c}_{d1}^{\mathrm{T}}\mathbf{b}_{d2}/(\mathbf{c}_{d2}^{\mathrm{T}}\mathbf{b}_{d2}) \tag{3.28}$$

$$\mathbf{c}_\chi = \mathbf{c}_{d1} - \chi\mathbf{c}_{d2}. \tag{3.29}$$

Substituting (3.8), (3.12), (3.20), and (3.27) into the time derivative of (3.22) yields

$$\frac{\mathbf{v}_{qds} - r_s\mathbf{i}_{qds} - \omega_r\boldsymbol{\lambda}_{dqs} - p\boldsymbol{\lambda}_{mqd}}{L_{ls}} = \boldsymbol{\Gamma}_{mi}(\boldsymbol{\lambda}_{mqd})p\boldsymbol{\lambda}_{mqd} + \begin{bmatrix} \mathbf{c}_q^{\mathrm{T}}\mathbf{A}_q(\mathbf{z}_q + \mathbf{b}_q\lambda_{mq}) + \mathbf{c}_q^{\mathrm{T}}\mathbf{b}_q p\lambda_{mq}) \\ \mathbf{c}_\chi^{\mathrm{T}}\mathbf{A}_d(\mathbf{z}_d + \mathbf{b}_{d1}\lambda_{md}) + \mathbf{c}_\chi^{\mathrm{T}}\mathbf{b}_{d1}p\lambda_{md} + \chi p i_{fdr} \end{bmatrix}. \quad (3.30)$$

Collecting terms that include $p\boldsymbol{\lambda}_{mqd}$ gives

$$\underbrace{\left(\frac{1}{L_{ls}}\mathbf{I}_2 + \begin{bmatrix} \mathbf{c}_q^{\mathrm{T}}\mathbf{b}_q & 0 \\ 0 & \mathbf{c}_\chi^{\mathrm{T}}\mathbf{b}_{d1} \end{bmatrix} + \boldsymbol{\Gamma}_{mi}(\boldsymbol{\lambda}_{mqd})\right)}_{\mathbf{L}_{mi}^{-1}} p\boldsymbol{\lambda}_{mqd} = - \underbrace{\left(\begin{bmatrix} \mathbf{c}_q^{\mathrm{T}}\mathbf{A}_q(\mathbf{z}_q + \mathbf{b}_q\lambda_{mq}) \\ \mathbf{c}_\chi^{\mathrm{T}}\mathbf{A}_d(\mathbf{z}_d + \mathbf{b}_{d1}\lambda_{md}) \end{bmatrix} - \frac{\mathbf{v}_{qds} - r_s\mathbf{i}_{qds} - \omega_r\boldsymbol{\lambda}_{dqs}}{L_{ls}}\right)}_{\boldsymbol{\xi}(\cdot)} - \begin{bmatrix} 0 \\ \chi p i_{fdr} \end{bmatrix} \quad (3.31)$$

where the matrix coefficient multiplying $p\boldsymbol{\lambda}_{mqd}$ is the inverse of the incremental inductance matrix $\mathbf{L}_{mi}$. The elements of $\mathbf{L}_{mi}$ are defined as

$$\mathbf{L}_{mi}(\boldsymbol{\lambda}_{mqd}) = \begin{bmatrix} L_{mqq} & L_{mqd} \\ L_{mqd} & L_{mdd} \end{bmatrix}. \quad (3.32)$$

and this matrix is symmetric because $\boldsymbol{\Gamma}_{mi}(\cdot)$ is required to be symmetric since a lossless coupling field is assumed. Left multiplying (3.31) by $\mathbf{L}_{mi}$ yields

$$p\boldsymbol{\lambda}_{mqd} = -\mathbf{L}_{mi}\left(\begin{bmatrix} 0 \\ \chi \end{bmatrix} p i_{fdr} + \boldsymbol{\xi}(\cdot)\right) \quad (3.33)$$

The term $\boldsymbol{\xi}$ defined in (3.31) can be partitioned such that

$$\boldsymbol{\xi}(\cdot) = \begin{bmatrix} \xi_q \\ \xi_d \end{bmatrix}. \quad (3.34)$$

Substituting (3.24) into (3.23) and substituting into the definition of ξ_d yields

$$\begin{aligned} \xi_d &= \left(\frac{1}{(\mathbf{c}_{d2})_1}\mathbf{c}_\chi^{\mathrm{T}}\mathbf{a}_{d1}\right) i_{fdr} + \mathbf{c}_\chi^{\mathrm{T}}\Bigg[(\bar{\mathbf{A}}_d - \frac{1}{(\mathbf{c}_{d2})_1}\mathbf{a}_{d1}\bar{\mathbf{c}}_{d2}^{\mathrm{T}})\bar{\mathbf{z}}_d \\ &\quad + (\mathbf{A}_d\mathbf{b}_{d1} - \frac{1}{(\mathbf{c}_{d2})_1}\mathbf{a}_{d1}\mathbf{c}_{d2}^{\mathrm{T}}\mathbf{b}_{d1})\lambda_{md}\Bigg] - \frac{\mathbf{v}_{ds} - r_s\mathbf{i}_{ds} + \omega_r\boldsymbol{\lambda}_{qs}}{L_{ls}} \\ &= a_f i_{fdr} + \bar{\xi}_d \end{aligned} \quad (3.35)$$

Substituting (3.35) into (3.33) gives

$$p\lambda_{md} = -L_{mqd}\xi_q - L_{mdd}(\chi p i_{fdr} + a_f i_{fdr} + \bar{\xi}_d) \quad (3.36)$$

and substituting with (3.23) and (3.24) into (3.21) yields

$$\begin{aligned} v_{fdr} &= \{p i_{fdr} - \mathbf{c}_{d2}^{\mathrm{T}}[\mathbf{a}_{d1}/(\mathbf{c}_{d2})_1(i_{fdr} - \bar{\mathbf{c}}_{d2}^{\mathrm{T}}\bar{\mathbf{z}}_d - \mathbf{c}_{d2}^{\mathrm{T}}\mathbf{b}_{d1}\lambda_{md}) \\ &\quad + \bar{\mathbf{A}}_d\bar{\mathbf{z}}_d + \mathbf{A}_d\mathbf{b}_{d1}\lambda_{md} + \mathbf{b}_{d1}(-L_{mqd}\xi_q \\ &\quad - L_{mdd}\{\chi p i_{fdr} + a_f i_{fdr} + \bar{\xi}_d\})]\}/(\mathbf{c}_{d2}^{\mathrm{T}}\mathbf{b}_{d2}) \\ &= r_{fdr} i_{fdr} + L_{fdr} p i_{fdr} + e_{fdr} \end{aligned} \quad (3.37)$$

where

$$\begin{aligned} r_{fdr} &= -\mathbf{c}_{d2}^{\mathrm{T}}(\mathbf{a}_{d1}/(\mathbf{c}_{d2})_1 - \mathbf{b}_{d1}L_{mdd}a_f)/(\mathbf{c}_{d2}^{\mathrm{T}}\mathbf{b}_{d2}) \\ &= r_{sfdr} - L_{mdd}a_f\sigma \end{aligned} \tag{3.38}$$

$$\begin{aligned} L_{fdr} &= (1 + \mathbf{c}_{d2}^{\mathrm{T}}\mathbf{b}_{d1}L_{mdd}\chi)/(\mathbf{c}_{d2}^{\mathrm{T}}\mathbf{b}_{d2}) \\ &= L_{sfdr} - L_{mdd}\chi\sigma \end{aligned} \tag{3.39}$$

$$\begin{aligned} e_{fdr} &= \mathbf{c}_{d2}^{\mathrm{T}}[(\mathbf{a}_{d1}\bar{c}_{d2}^{\mathrm{T}}/(\mathbf{c}_{d2})_1 - \bar{\mathbf{A}}_d)\bar{\mathbf{z}}_d \\ &\quad + (\mathbf{a}_{d1}\mathbf{c}_{d2}^{\mathrm{T}}\mathbf{b}_{d1}/(\mathbf{c}_{d2})_1 - \mathbf{A}_d\mathbf{b}_{d1})\lambda_{md} \\ &\quad + \mathbf{b}_{d1}(L_{mqd}\xi_q + L_{mdd}\bar{\xi}_d)\ ]/(\mathbf{c}_{d2}^{\mathrm{T}}\mathbf{b}_{d2}) \end{aligned} \tag{3.40}$$

where

$$r_{sfdr} = (-\mathbf{c}_{d2}^{\mathrm{T}}\mathbf{a}_{d1}/(\mathbf{c}_{d2})_1)/(\mathbf{c}_{d2}^{\mathrm{T}}\mathbf{b}_{d2}) \tag{3.41}$$

$$L_{sfdr} = 1/(\mathbf{c}_{d2}^{\mathrm{T}}\mathbf{b}_{d2}) \tag{3.42}$$

$$\sigma = -\mathbf{c}_{d2}^{\mathrm{T}}\mathbf{b}_{d1}/(\mathbf{c}_{d2}^{\mathrm{T}}\mathbf{b}_{d2}) \tag{3.43}$$

3.4 Model Summary

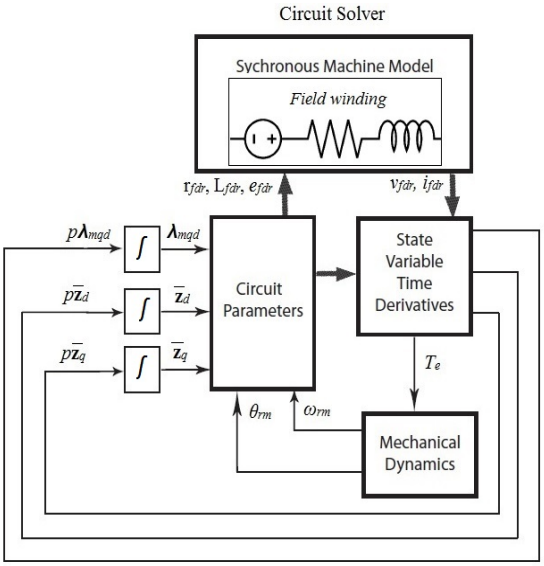

Figure 3.1: Model structure summary

The proposed model can be thought to function in three stages. The overall model structure is depicted in Figure 3.1. In the first stage, the values of the state variables at time t (θ_{rm}, ω_{rm}, $\boldsymbol{\lambda}_{mqd}$, $\bar{\mathbf{z}}_d$ and $\mathbf{z}_q$) are used to calculate circuit parameters:

1. Compute ω_r from (3.4).
2. Compute $\hat{\lambda}_m$ from (3.11) and $\Gamma_{mq}(\hat{\lambda}_m)$ and $\Gamma_{md}(\hat{\lambda}_m)$ from their definitions.
3. Compute $\boldsymbol{\Gamma}_{mi}$ from (3.13).
4. Calculate $\mathbf{i}_{mqd}$ from (3.9) and (3.10)
5. Calculate $\mathbf{i}_{qdr}$ from (3.17) and (3.26)

6. Calculate $\mathbf{i}_{qds}$ from (3.22) and $\boldsymbol{\lambda}_{qds}$ from (3.7)
7. Transform $\mathbf{i}_{qd0s}$ from the rotating reference frame with the inverse of (3.1)
8. Compute $\mathbf{v}_{abcs}$ from the stator circuitry model
9. Transform $\mathbf{v}_{abcs}$ to the rotating reference frame using (3.1)
10. Compute $\mathbf{L}_{mi}$ from its definition in (3.31), and extract the elements L_{mqd}, and L_{mdd} from their definition in (3.32).
11. Compute ξ_q and $\bar{\xi}_d$ from their definitions in (3.31) and (3.35) respectively
12. Compute r_{fdr}, L_{fdr} and e_{fdr} from their definitions in (3.38)-(3.40)

In the second stage, the circuit parameters are combined with circuit representations of the interconnected equipment. This system is solved using a circuit solver to calculate v_{fdr} and i_{fdr}. In the third stage, the voltages and currents from the circuit solver are used to calculate the time derivatives of the state variables:

1. Compute z_{d1} from (3.24).
2. Compute $p\mathbf{z}_d$ and $p\mathbf{z}_q$ from (3.14) and (3.16), respectively, and extract $p\bar{\mathbf{z}}_d$.
3. Compute ξ from its definition in (3.31).
4. Solve (3.21) for pi_{fdr}.
5. Compute $p\boldsymbol{\lambda}_{mqd}$ from (3.33).
6. The time derivatives of the mechanical state variables (θ_{rm} and ω_{rm}) are computed using the prime mover model. The torque developed by the synchronous machine is given by [24]

$$T_e = \frac{3}{2}\frac{P}{2}(i_{qs}\lambda_{md} - i_{ds}\lambda_{mq}). \tag{3.44}$$

3.5 FVBR Studies

In this section, the proposed model is compared with the previous SFVBR model [25].The main machine spins at 1800 r/min and is feeding a purely resistive load. The load resistance is 50 Ω. All simulations are performed using Simulink's ode23tb integration algorithm with a maximum time step of 0.167 ms, and a relative tolerance of 10^{-3}. ASMG is used for circuit simulation [36].
When the load (50 Ω) is applied, a main field voltage as shown in Figure 3.2 is applied, since both of the FVBR and SFVBR models use the same brushless exciter model, the main field voltage applied should be the same.

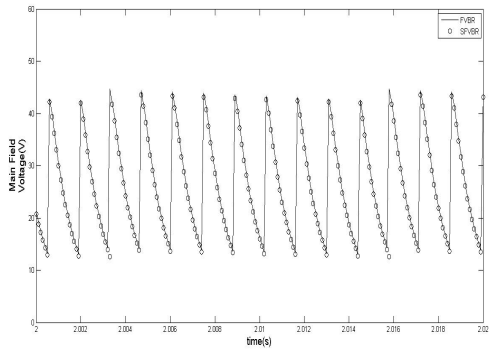

Figure 3.2: Main machine field voltage.

Both models are implemented for the same synchronous machine, and identical loads are applied,therefore, the machine outputs in both models are expected to be the same. This can be shown in Figure 3.3.

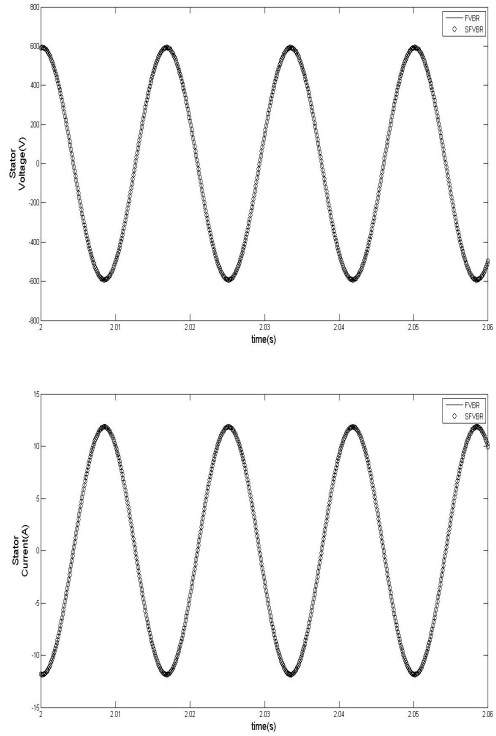

Figure 3.3: Top: *as* line-to-ground voltage. Bottom: *as* line current

Chapter 4

Brushless Exciter Model

A brushless exciter model is formulated in a VBR form to be compatible with the proposed average-value model, where the exciter open-circuit subtransient voltages are available to be used as inputs to the AVM in order to define the dynamic impedance. The model set forth is similar to the VBR model presented in [37]. It has been modified to account for the fact that the field winding is on the stator and the armature windings are on the rotor.
Magnetic saturation or arbitrary network representations are not included. A residual flux term (represented by λ_{md0}) has been included in the d-axis magnetizing flux in order to account for the effects of magnetic hysteresis. The parameters of the model are provided in Table 7.2.
The exciter voltage equations can be expressed in the stator reference frame by

$$v^s_{qr} = r_r i^s_{qr} - \omega_r \lambda^s_{dr} + p\lambda^s_{qr} \tag{4.1}$$
$$v^s_{dr} = r_r i^s_{dr} + \omega_r \lambda^s_{qr} + p\lambda^s_{dr} \tag{4.2}$$
$$v^{'}_{fds} = r^{'}_{fds} i^{'}_{fds} + p\lambda^{'}_{fds} \tag{4.3}$$

The rotor flux linkages can be divided into a leakage term and a magnetizing term:

$$\boldsymbol{\lambda}^s_{qdr} = L_{lr}\mathbf{i}^s_{qdr} + \boldsymbol{\lambda}_{mqd} \tag{4.4}$$

where L_{lr} is the rotor leakage inductance and $\boldsymbol{\lambda}_{mqd}$ are the magnetizing flux linkages which are given by

$$\lambda_{mq} = L_{mq} i^s_{qr} \tag{4.5}$$
$$\lambda_{md} = L_{md}(i^s_{dr} + i^{'}_{fds}) + \lambda_{md0}. \tag{4.6}$$

The stator flux linkage can be expressed as

$$\lambda^{'}_{fds} = L^{'}_{lfds} i^{'}_{fds} + \lambda_{md}. \tag{4.7}$$

Solving (4.7) for $i^{'}_{fds}$ yields

$$i^{'}_{fds} = \frac{\lambda^{'}_{fds} - \lambda_{md}}{L^{'}_{lfds}} \tag{4.8}$$

and substituting (4.8) into (4.6) gives

$$\lambda_{md} = L^{''}_{md}(i^s_{dr} + \frac{\lambda^{'}_{fds}}{L^{'}_{lfds}}) + \frac{L^{''}_{md}}{L_{md}}\lambda_{md0} \tag{4.9}$$

where

$$L^{''}_{md} = \frac{1}{\frac{1}{L_{md}} + \frac{1}{L^{'}_{lfds}}} \tag{4.10}$$

substituting (4.5) and (4.9) into (4.4) gives, after algebraic manipulation,

$$\lambda^s_{qr} = L^{''}_q i^s_{qr} \tag{4.11}$$

$$\lambda^s_{dr} = L^{''}_d i^s_{dr} + \lambda^{''}_d \tag{4.12}$$

where

$$L^{''}_q = L_{lr} + L_{mq} \tag{4.13}$$

$$= L_{lr} + L^{''}_{mq} \tag{4.14}$$

$$L^{''}_d = L_{lr} + L^{''}_{md} \tag{4.15}$$

$$\lambda^{''}_d = \frac{L^{''}_{md}}{L^{'}_{lfds}} \lambda^{'}_{fds} + \frac{L^{''}_{md}}{L_{md}} \lambda_{md0} \tag{4.16}$$

Substituting (4.11) and (4.12) into (4.1) and (4.2), the rotor voltage equations may be rewritten as

$$v^s_{qr} = r_r i^s_{qr} - \omega_r (L^{''}_d i^s_{dr} + \lambda^{''}_d) + p(L^{''}_q i^s_{qr}) \tag{4.17}$$

$$v^s_{dr} = r_r i^s_{dr} + \omega_r (L^{''}_q i^s_{qr}) + p(L^{''}_d i^s_{dr} + \lambda^{''}_d) \tag{4.18}$$

Solving (4.3) for $p\lambda^{'}_{fds}$ and substituting (4.8) into the resulting expression yields

$$p\lambda^{'}_{fds} = v^{'}_{fds} - r^{'}_{fds} \left(\frac{\lambda^{'}_{fds} - L^{''}_{md} i^s_{dr} - \lambda^{''}_d}{L^{'}_{lfds}} \right) \tag{4.19}$$

Substituting (4.19) into the time derivative of (4.16) and substituting into (4.18) gives the rotor voltage equations

$$\begin{aligned} v_{qr}^{s} &= r_r i_{qr}^{s} - \omega_r L_d^{''} i_{dr}^{s} - \omega_r \lambda_d^{''} + p(L_q^{''} i_{qr}^{s}) \\ &= r_q^{''} i_{qr}^{s} - \omega_r L_d^{''} i_{dr}^{s} + p(L_q^{''} i_{qr}^{s}) + e_q^{''} \qquad (4.20) \\ v_{dr}^{s} &= r_r i_{dr}^{s} + \omega_r L_q^{''} i_{qr}^{s} + p L_d^{''} i_{dr}^{s} \\ &\quad + \frac{L_{md}^{''}}{L_{fds}^{'}}(v_{fds}^{'} - r_{fds}^{'}(\frac{\lambda_{fds}^{'} - L_{md}^{''} i_{dr}^{s} - \lambda_d^{''}}{L_{lfds}^{'}})) \\ &= r_d^{''} i_{dr}^{s} + \omega_r L_q^{''} i_{qr}^{s} + p L_d^{''} i_{dr}^{s} + e_d^{''} \qquad (4.21) \end{aligned}$$

where

$$r_q^{''} = r_r \qquad (4.22)$$

$$r_d^{''} = r_r + \frac{L_{md}^{''2} r_{fds}^{'}}{L_{lfds}^{'2}} \qquad (4.23)$$

$$e_q^{''} = -\omega_r \lambda_d^{''} \qquad (4.24)$$

$$e_d^{''} = \frac{L_{md}^{''}}{L_{lfds}^{'}} v_{fds}^{'} + \frac{L_{md}^{''} r_{fds}^{'}}{L_{lfds}^{'2}}(\lambda_d^{''} - \lambda_{fds}^{'}) \qquad (4.25)$$

Chapter 5

Average Value Model

A detailed simulation which includes synchronous machine dynamics and semiconductor switching states yields accurate results; however, detailed computer simulations are computationally intensive since the switching of each semiconductor must be taken into account.
To overcome this problem an average-value model of the rotating rectifier feeding the main machine field circuit in a brushless excitation system is set forth. The approach presented in this study extends the work of [34], it requires a detailed simulation for extracting the essential AVM parameters.
In the proposed model, the rectifier dc variables are averaged over the switching interval and then related to the brushless exciter currents and voltages expressed in the qd form through the extracted parameters, these relationships can be approximated as

$$\left|\left|\bar{\mathbf{v}}^s_{qdr}\right|\right| = \alpha(\cdot)\bar{v}_{fdr} \tag{5.1}$$

$$\bar{i}_{fdr} = \beta(\cdot)\left|\left|\bar{\mathbf{i}}^s_{qdr}\right|\right| \tag{5.2}$$

From Figure 5.1 the angle between the exciter voltage and current vectors can be expressed as

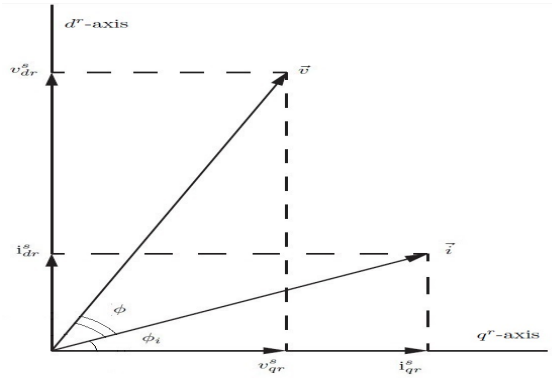

Figure 5.1: Relationship between the exciter voltages and currents vectors.

$$\begin{aligned}\phi(\cdot) &= \angle(\bar{v}^s_{qr} + j\bar{v}^s_{dr}) - \angle(\bar{i}^s_{qr} + j\bar{i}^s_{dr}) \\ &= \arctan\left(\frac{\bar{v}^s_{dr}}{\bar{v}^s_{qr}}\right) - \arctan\left(\frac{\bar{i}^s_{dr}}{\bar{i}^s_{qr}}\right)\end{aligned} \tag{5.3}$$

The exciter and the AVM of the rectifier are shown in Figure 5.2, the rectifier is represented by an algebraic block that outputs the averaged main field voltage and exciter currents, whereas the inputs to that block are the main field current and exciter internal voltages.

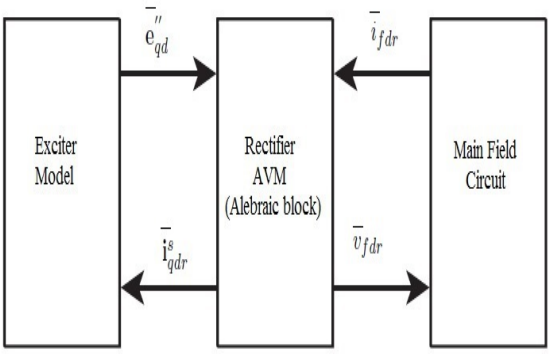

Figure 5.2: Average-value modeling.

The functions $\alpha(\cdot)$, $\beta(\cdot)$, and $\phi(\cdot)$ are algebraic functions of the loading conditions that can be accounted for by introducing an impedance, such impedance can be defined as

$$z = \frac{\left|\left|\bar{\mathbf{e}}''_{qd}\right|\right|}{\bar{i}_{fdr}} \tag{5.4}$$

The detailed model described in chapter 3 has been used to compute $\alpha(z)$, $\beta(z)$, and $\phi(z)$ according to (5.1)-(5.3). The resulting functions are plotted in Figure 5.3. The data points that are used to produce these functions are given in the appendix.

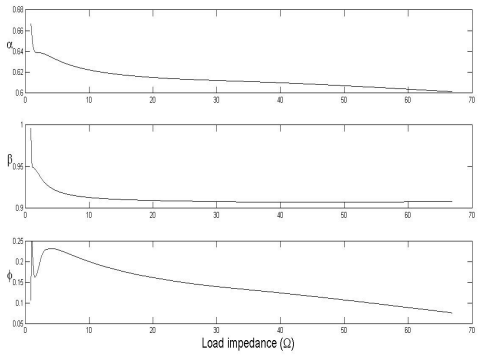

Figure 5.3: Functions α, β, and ϕ obtained from the detailed model.

The main machine has been connected to a resistive load, and the exciter field voltage has been varied in a wide range to vary the loading conditions in order to ensure that the parameters $\alpha(z)$, $\beta(z)$, and $\phi(z)$ are valid for various operating conditions.The block diagram depicted in Figure 5.4 shows the structure of the proposed AVM.

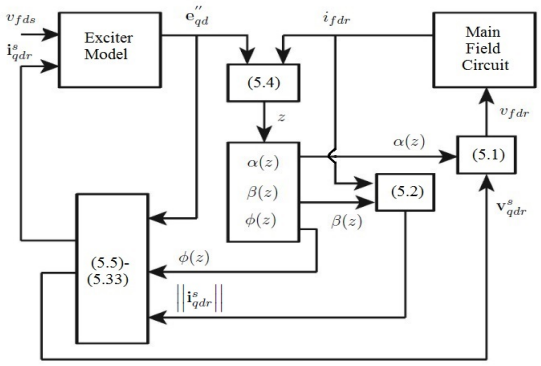

Figure 5.4: Structure of the proposed AVM.

A state model for the exciter is proposed where the rotor currents and their time derivatives are the inputs and outputs respectively

$$p\mathbf{x} = \mathbf{A}\mathbf{x} + \mathbf{B}\mathbf{i}^s_{qdr} \tag{5.5}$$

$$p\mathbf{i}^s_{qdr} \approx \mathbf{C}\mathbf{x} + \mathbf{D}\mathbf{i}^s_{qdr} \tag{5.6}$$

Ideally, the transfer function of such a system can be given by

$$\mathbf{H}(s) = s\mathbf{I} \tag{5.7}$$

From (5.6) appropriate expressions for the time derivatives of the rotor currents can be obtained by selecting the elements of D, which can then be substituted into the rotor voltage equations to make the calculation of the remaining unknowns possible as shown later.
The matrix $\mathbf{D}$ is selected such that

$$\mathrm{D}_{11} = \frac{\Delta r}{L''_q} + \delta \tag{5.8}$$

$$\mathrm{D}_{22} = \frac{L''_q}{L''_d}\delta \tag{5.9}$$

$$\mathrm{D}_{12} = \frac{-\omega^*_r \Delta L}{L''_q + L''_d} \tag{5.10}$$

$$\mathrm{D}_{21} = \mathrm{D}_{12} \tag{5.11}$$

where

$$\Delta r = r''_d - r''_q \tag{5.12}$$

$$\Delta L = L''_d - L''_q \tag{5.13}$$

$$\delta = 1 \times 10^5 \tag{5.14}$$

And ω^*_r is the nominal electrical angular velocity.
The matrices $\mathbf{A}$, $\mathbf{B}$, and $\mathbf{C}$ are specified as

$$\mathbf{A} = -\mathbf{\Lambda} \tag{5.15}$$

$$\mathbf{B} = \mathbf{V}^{-1} \tag{5.16}$$

$$\mathbf{C} = -\mathbf{V}\mathbf{\Lambda}^2 \tag{5.17}$$

where $\mathbf{V}$ is a matrix whose columns are the eigenvectors of $\mathbf{D}$, and $\mathbf{\Lambda}$ is a diagonal matrix containing the eigenvalues of $\mathbf{D}$ along the main diagonal.
The matrices $\mathbf{A}$, $\mathbf{B}$, $\mathbf{C}$ and $\mathbf{D}$ are selected in that way to ensure that the transfer function of the proposed state model satisfies the following condition in order to approximate a time derivative

$$\lim_{s\to 0} \frac{\tilde{\mathbf{H}}(s)}{s} = \mathbf{I} \tag{5.18}$$

The proof of (5.18) is provided in the appendix.

The exciter rotor equations (4.20) and (4.21) can be rewritten as

$$v_{qr}^{s} = r_{q}^{''} i_{qr}^{s} - \omega_r L_{q}^{''} i_{dr}^{s} + p(L_{q}^{''} i_{qr}^{s}) + e_{q}^{''} - \omega_r (L_{d}^{''} - L_{q}^{''}) i_{dr}^{s} \tag{5.19}$$

$$v_{dr}^{s} = r_{q}^{''} i_{dr}^{s} + \omega_r L_{q}^{''} i_{qr}^{s} + p(L_{d}^{''} i_{dr}^{s}) + e_{d}^{''} + (r_{d}^{''} - r_{q}^{''}) i_{dr}^{s} \tag{5.20}$$

Substituting the time derivatives of the exciter rotor currents from (5.6) into (5.19) and (5.20) yields after algebraic manipulation

$$v_{qr}^{s} = (r_{q}^{''} + R) i_{qr}^{s} - (\omega_r L_{q}^{''} + X) i_{dr}^{s} + f_q \tag{5.21}$$

$$v_{dr}^{s} = (r_{q}^{''} + R) i_{dr}^{s} + (\omega_r L_{q}^{''} + X) i_{qr}^{s} + f_d \tag{5.22}$$

where

$$\begin{aligned} R &= L_{q}^{''} \mathrm{D}_{11} \\ &= L_{d}^{''} \mathrm{D}_{22} + (r_{d}^{''} - r_{q}^{''}) \end{aligned} \tag{5.23}$$

$$\begin{aligned} X &= L_{d}^{''} \mathrm{D}_{21} \\ &= \omega_r (L_{d}^{''} - L_{q}^{''}) - L_{q}^{''} \mathrm{D}_{12} \end{aligned} \tag{5.24}$$

$$f_q = L_{q}^{''} \mathrm{C}_{11} \mathrm{x}_1 + L_{q}^{''} \mathrm{C}_{12} \mathrm{x}_2 + e_{q}^{''} \tag{5.25}$$

$$f_d = L_{d}^{''} \mathrm{C}_{21} \mathrm{x}_1 + L_{d}^{''} \mathrm{C}_{22} \mathrm{x}_2 + e_{d}^{''} \tag{5.26}$$

Each of the parameters R and X has two equivalent expressions due to the proper selection of the $\mathbf{D}$ matrix elements based on (5.8)-(5.11), as a result the $q-$ and $d-$axis voltages in (5.21) and (5.22) have identical current coefficients, which makes it possible now to calculate the unknown voltage magnitude and phase angle.
The vector $\mathbf{v}_{qdr}^{s}$ can be expressed as

$$\begin{aligned} \vec{v} &= v_{qr}^{s} + j v_{dr}^{s} \\ &= V_p \angle(\phi + \phi_i) \end{aligned} \tag{5.27}$$

Substituting (5.21) and (5.22) in (5.27) gives

$$\begin{aligned} \vec{v} &= (r_{q}^{''} + R)(i_{qr}^{s} + j i_{dr}^{s}) + j(\omega_r L_{q}^{''} + X)(i_{qr}^{s} + j i_{dr}^{s}) + f_q + j f_d \\ &= Z\vec{i} + \vec{f} \end{aligned} \tag{5.28}$$

where

$$\vec{i} = \mathrm{i}_{qr}^{s} + j \mathrm{i}_{dr}^{s} \tag{5.29}$$

$$= I_p \angle \phi_i \tag{5.30}$$

$$Z = r_{q}^{''} + R + j(\omega_r L_{q}^{''} + X) \tag{5.31}$$

$$\vec{f} = f_q + j f_d \tag{5.32}$$

Rewriting (5.28) in the complex exponential form

$$\mathrm{V}_p e^{j(\phi + \phi_i)} = Z I_p e^{j(\phi_i + \pi)} + \vec{f} \tag{5.33}$$

Solving (5.33) for V_p and ϕ_i yields

$$V_p = \sqrt{\left|\left|\vec{f}\right|\right|^2 - (\mathrm{Im}(Z I_p e^{-j\phi}))^2} - \mathrm{Re}(Z I_p e^{-j\phi}) \tag{5.34}$$

$$\phi_i = \angle \frac{\vec{f}}{V_p e^{j\phi} + Z I_p} \tag{5.35}$$

Chapter 6

Average-Value-Model Studies

In the following study, the detailed simulation is compared with the responses generated by the AVM. The system operates with a constant excitation of 12.0 V and a load resistance of 5.31 Ω connected to the main machine stator phases.
In Figure 6.1, the voltages and currents that the rotating rectifier feeds to the main machine field circuit are shown in both AVM and detailed simulations. As can be seen, the main field voltage in the AVM is approximately equal to the average value of the detailed field voltage, and the AVM field current follows almost exactly the path produced by the detailed model.
The output waveforms from both models are also compared. An excellent agreement between the detailed and AVM simulation waveforms can be shown in Figure 6.2.
At time t=1.0 s, the load resistance is increased from 1 Ω to 30 Ω, and the exciter field voltage is reduced from 30 V to 10 V. In Figure 6.3, the transient observed in the phase a exciter current is predicted using the detailed simulation.Therein, it is shown that the current i_{ar} is discontinuous and ,thus, the rectifier operates in mode 1. In Figure 6.4, the detailed simulation is compared with response generated by the AVM. As can be seen, the AVM response follows both the general transient and steady-sate very well.
In order to drive the rotating rectifier into mode 2, at time t=1.75 s, the load resistance is reduced from 5.31 Ω to 2 Ω, The simulated phase a exciter current is shown in Figure 6.5. Therein, it is shown that i_{ar} is continuous which indicates the mode 2 operation. The detailed and AVM system responses to that load step change are shown in Figure 6.6, it is shown that the field current response of the averaged model follows exactly the current trace produced by the detailed simulation during both the transient and steady-state response, while the voltage response of the AVM follows almost exactly the average value of detailed field voltage in steady-state, however, it does not capture the transient characteristics accurately.

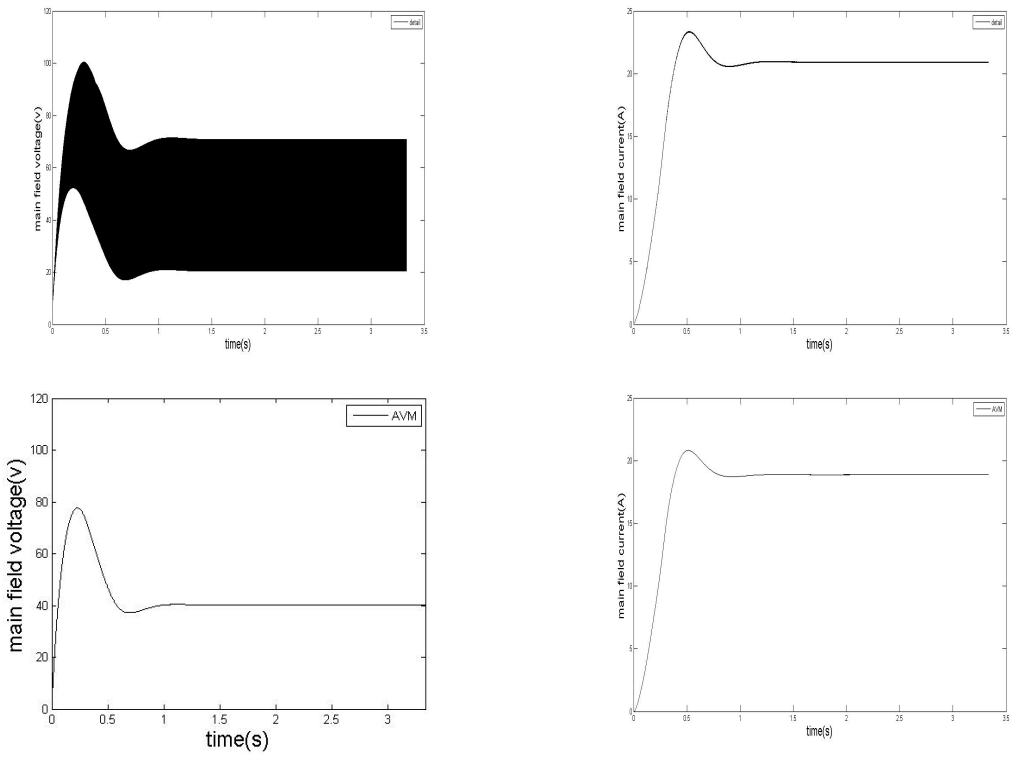

Figure 6.1: System response; detailed and AVM

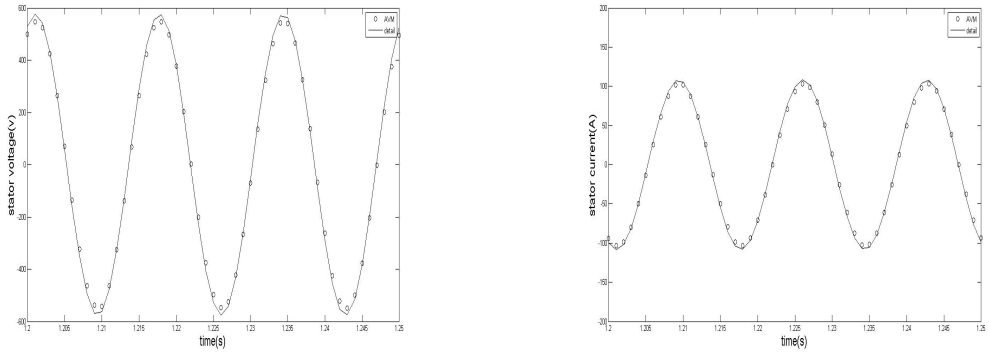

Figure 6.2: Output voltage and current; detailed and AVM

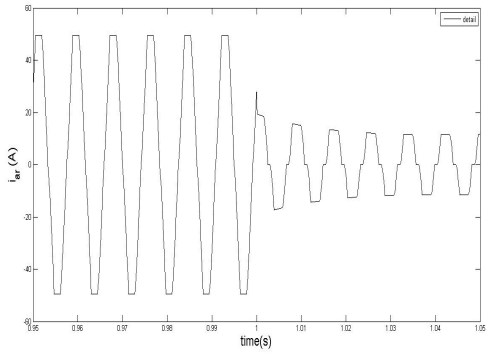

Figure 6.3: Simulated response to a load step change in mode 1; exciter ac current

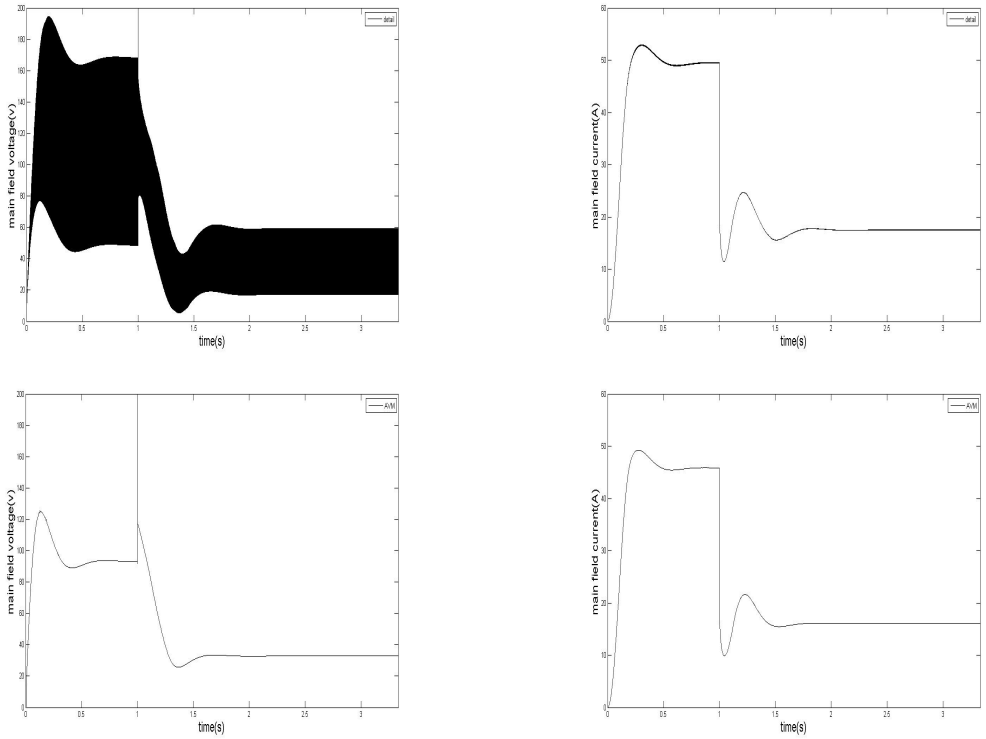

Figure 6.4: System response to a load step change in mode 1; detailed and AVM

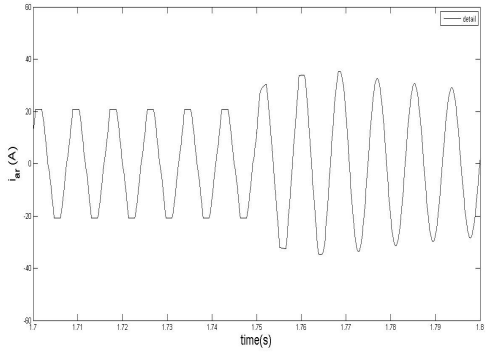

Figure 6.5: Simulated response to a load step change in mode 2; exciter ac current

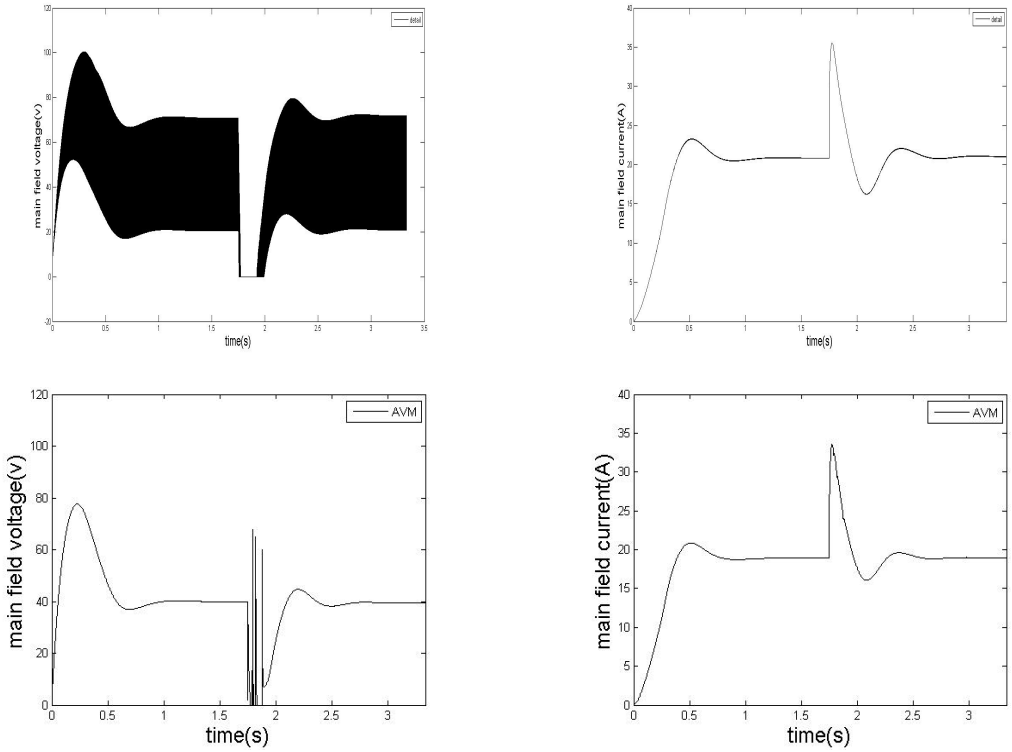

Figure 6.6: System response to a load step change in mode 2; detailed and AVM

Chapter 7

Conclusion

A VBR reformulation of the detailed synchronous machine model of [25] is presented, since the rotating rectifier connected to the main machine field circuit in a brushless excitation system is of interest, a VBR representation for the field winding of the main synchronous generator is set forth. The FVBR model is validated by comparison with the previous SFVBR model, the simulation results of both models are essentially identical; this is because the two models are mathematically equivalent. The FVBR model is less versatile and less flexible reformulation of the SFVBR model because in this study the focus is on the field side only of the main machine.
An average-value model for the rotating rectifier is also presented; this model largely follows the AVM set forth in [34], where the relationship between the rectifier averaged dc variables and the exciter currents and voltages expressed in the stator frame of reference is defined by parameters that vary depending on the loading conditions, a detailed simulation is required to extract these parameters and build the averaged model.The brushless exciter is implemented in an appropriate VBR model form using the classical qd formulation to be compatible with the proposed averaged model.
The resulting AVM is verified against detailed simulation, where the simulation results of the AVM agree very well with those of the detailed simulation.

Appendix

Main Machine and Exciter Parameters

The main machine used in this study is 59-kW, 560-V. The machine parameters are obtained from [22]. Some of the parameters of the model are provided in Table 7.1. The d-axis inverse magnetizing inductance is

$$\Gamma_{md}(\hat{\lambda}_m) = 10^3 \cdot \frac{1 - 1.122\hat{\lambda}_m + 0.3348\hat{\lambda}_m^2}{29.20 - 32.48\hat{\lambda}_m + 9.261\hat{\lambda}_m^2} \tag{7.1}$$

for $\hat{\lambda}_m \leq \hat{\lambda}_{m1}$. Otherwise,

$$\Gamma_{md}(\hat{\lambda}_m) = \frac{1}{L_{md,sat}} + \left[\Gamma_{md}(\hat{\lambda}_{m1}) - \frac{1}{L_{md,sat}}\right] \frac{\hat{\lambda}_{m1}}{\hat{\lambda}_m}. \tag{7.2}$$

The q-axis inverse magnetizing inductance is

$$\Gamma_{mq}(\hat{\lambda}_m) = \alpha\Gamma_{md}(\hat{\lambda}_m) + \beta. \tag{7.3}$$

The d-axis rotor network matrices are transformed such that $(\mathbf{c}_{d1})_1 = 0$

$$\mathbf{A}_d = \begin{bmatrix} 9.920 \times 10^2 & 1.580 \times 10^2 & -8.430 \times 10^2 \\ -1.198 \times 10^4 & -1.849 \times 10^3 & 6.457 \times 10^3 \\ -1.130 \times 10^2 & -1 \times 10^1 & -5.840 \times 10^2 \end{bmatrix} \tag{7.4}$$

$$\mathbf{B}_d = \begin{bmatrix} -1.326 \times 10^3 & 8.300 \times 10^1 \\ 1.440 \times 10^4 & -8.840 \times 10^2 \\ -7.060 \times 10^{-2} & 0 \end{bmatrix} \tag{7.5}$$

$$\mathbf{C}_d = \begin{bmatrix} 0 & 1 & -9.992 \times 10^{-15} \\ 1 & -5.204 \times 10^{-18} & 0 \end{bmatrix} \tag{7.6}$$

whereas the q-axis rotor network is characterized by

$$\mathbf{A}_q = \begin{bmatrix} -6.835 \times 10^2 & 0 \\ 0 & -1 \times 10^2 \end{bmatrix} \tag{7.7}$$

$$\mathbf{b}_q = \begin{bmatrix} 1 \\ 0 \end{bmatrix} \tag{7.8}$$

$$\mathbf{c}_q^{\mathrm{T}} = \begin{bmatrix} 3.978 \times 10^3 & 0 \end{bmatrix}. \tag{7.9}$$

Table 7.1: Main Machine Parameters

P	4	r_s	0.108 Ω
r_{fdr}	2.01 Ω	L_{ls}	0.97 mH
α	2.461	β	-6.580 H^{-1}
$L_{md,sat}$	2.9 mH	$\hat{\lambda}_{m1}$	1.6 Vs

Table 7.2: Brushless Exciter Parameters

P	8	N_r/N_{fds}	0.07
r_r	0.121 Ω	L_{lr}	0.49 mH
r_{fds}	4.69 Ω	L_{lfds}	0.117 H
L_{mq}	1.82 mH	L_{md}	3.49 mH
λ_{md0}	5.69 mVs		

Proof

The transfer function of the exciter proposed state model can be written as

$$\tilde{\mathbf{H}}(s) = \mathbf{C}(s\mathbf{I} - \mathbf{A})^{-1}\mathbf{B} + \mathbf{D} \tag{7.10}$$

Substituting the matrices **A**, **B**, **C** and **D** in (7.10) yields

$$\begin{aligned}\tilde{\mathbf{H}}(s) &= -\mathbf{V}\mathbf{\Lambda}^2 \begin{bmatrix} s+\lambda_1 & 0 \\ 0 & s+\lambda_2 \end{bmatrix}^{-1} \mathbf{V}^{-1} + \mathbf{V}\mathbf{\Lambda}\mathbf{V}^{-1} \\ &= -\mathbf{V} \begin{bmatrix} \frac{\lambda_1^2}{s+\lambda_1} & 0 \\ 0 & \frac{\lambda_2^2}{s+\lambda_2} \end{bmatrix} \mathbf{V}^{-1} + \mathbf{V}\mathbf{\Lambda}\mathbf{V}^{-1} \end{aligned} \tag{7.11}$$

Adding the two terms in (7.11) gives

$$\tilde{\mathbf{H}}(s) = \mathbf{V} \begin{bmatrix} \frac{\lambda_1 s}{s+\lambda_1} & 0 \\ 0 & \frac{\lambda_2 s}{s+\lambda_2} \end{bmatrix} \mathbf{V}^{-1} \tag{7.12}$$

Lookup table

Table 7.3: Data points for $\alpha(z)$, $\beta(z)$, and $\phi(z)$

z	α	β	ϕ
0.8946	0.6664	0.9960	0.1059
1.2046	0.6463	0.9495	0.2053
1.6221	0.6394	0.9465	0.1630
2.1842	0.6387	0.9404	0.1900
2.9411	0.6378	0.9319	0.2247
3.9604	0.6350	0.9251	0.2309
5.3328	0.6310	0.9198	0.2274
7.1808	0.6268	0.9160	0.2165
9.6693	0.6228	0.9133	0.2016
13.0201	0.6192	0.9113	0.1853
17.5322	0.6162	0.9099	0.1682
23.6078	0.6137	0.9088	0.1518
31.7888	0.6118	0.9079	0.1363
42.8050	0.6092	0.9073	0.1192
57.6386	0.6046	0.9077	0.0929

Bibliography

[1] J. G. Ciezki and R. W. Ashton, "Selection and stability issues associated with a navy shipboard dc zonal electric distribution system," vol. 15, no. 2, pp. 665–669, Apr. 2000.

[2] J. G. Kettleborough, I. R. Smith, and B. A. Fanthome, "Simulation of a dedicated aircraft generator supplying a heavy rectified load," *IEE Proc. B, Electric Power Applicat.*, vol. 130, no. 6, pp. 431–435, Nov. 1983.

[3] T. H. Warner and J. G. Kassakian, "Transient characteristics of large turboalternator driven rectifier/inverter systems based on field test data," vol. PAS-104, no. 7, pp. 1804–1811, Jul. 1985.

[4] R. W. Ferguson, R. Herbst, and R. W. Miller, "Analytical studies of the brushless excitation system," vol. 78, no. 4, pp. 1815–1821, Feb. 1960.

[5] E. C. Whitney, D. B. Hoover, and P. O. Bobo, "An electric utility brushless excitation system," vol. 79, no. 3, pp. 1821–1828, Feb. 1960.

[6] T. Zouaghi and M. Poloujadoff, "Modeling of polyphase brushless exciter behavior for failing diode operation," vol. 13, no. 3, pp. 214–220, Sep. 1998.

[7] S. J. Chapman, *Electric Machinery Fundamentals*, 4th ed. Avenue of the Americas, NY: McGraw-Hill, 2005.

[8] J. J. Grainger and J. William D. Stevenson, *Power System Analysis*, international ed. Hightstown, NJ: McGraw-Hill, 1994.

[9] P. C. Krause, O. Wasynczuk, and S. D. Sudhoff, *Analysis of Electric Machinery and Drive Systems*, 2nd ed. Piscataway, NJ: IEEE Press, 2002.

[10] D. A. Neamen, *Microelectronics Circuit Analysis and Design*, 4th ed. Avenue of the Americas, NY: McGraw-Hill, 2009.

[11] M. H. Rshid, *Power Electronics Handbook*, 1st ed. San Diego, CA: Academic Press, 2001.

[12] R. L. Witzke, J. V. Kresser, and J. K. Dillard, "Influence of ac reactance on voltage regulation of 6-phase rectifiers," vol. 27, no. 3, pp. 244–253, Jul. 1953.

[13] MATLAB, *version 8.10.0 (R2013a)*. Natick, Massachusetts: The MathWorks Inc., 2013.

[14] I. M. Canay, "Determination of the model parameters of machines from the reactance operators $x_d(p)$, $x_q(p)$ (evaluation of standstill frequency response test)," vol. 8, no. 2, pp. 272–279, Jun. 1993.

[15] A. Keyhani and H. Tsai, "Identification of high-order synchronous generator models from SSFR test data," vol. 9, no. 3, pp. 593–603, Sep. 1994.

[16] M. Fadel, M. Hasni, O. Touhami, R. Ibtouen, and S. Caux, "Estimation of synchronous machine parameter by standstill frequency response tests," vol. 59, no. 2, pp. 75–80, 2008.

[17] H. Bissig, K. Reichert, and T. S. Kulig, "Modeling and identification of synchronous machines, a new approach with an extended frequency range," vol. 8, no. 2, pp. 263–271, Jun. 1993.

[18] J. Verbeeck, R. Pintelon, and P. Guillaume, "Determination of synchronous machine parameters using network synthesis techniques," vol. 14, no. 3, pp. 310–314, Sep. 1999.

[19] L. Salvatore and M. Savino, "Experimental determination of synchronous machine parameters," vol. 128, no. 4, pp. 212–218, Jul. 1981.

[20] I. M. Canay, "Modeling of alternating-current machines having multiple rotor circuits," vol. 8, no. 2, pp. 280–296, Jun. 1993.

[21] D. C. Aliprantis, S. D. Sudhoff, and B. T. Kuhn, "A synchronous machine model with saturation and arbitrary rotor network representation," vol. 20, no. 3, pp. 584–594, Sep. 2005.

[22] ——, "Experimental characterization procedure for a synchronous machine model with saturation and arbitrary rotor network representation," vol. 20, no. 3, pp. 595–603, Sep. 2005.

[23] S. D. Sudhoff, D. C. Aliprantis, B. T. Kuhn, and P. L. Chapman, "An induction machine model for predicting inverter-machine interaction," vol. 17, no. 2, pp. 203–210, Jun. 2002.

[24] D. C. Aliprantis, O. Wasynczuk, and C. D. Rodríguez Valdez, "A voltage-behind-reactance synchronous machine model with saturation and arbitrary rotor network representation," vol. 23, no. 2, pp. 499–508, Jun. 2008.

[25] A. M. Cramer, D. C. Aliprantis, and B. P. Loop, "Synchronous machine model with voltage-behind-reactance formulation of stator and field windings," vol. 27, no. 2, pp. 499–508, Jun. 2012.

[26] H. A. Peterson and P. C. Krause, "A direct- and quadrature-axis representation of a parallel ac nd dc power system," vol. 85, no. 3, pp. 210–225, Mar. 1966.

[27] P. C. Krause and T. A. Lipo, "Analysis and simplified representation of a rectifier-inverter induction motor drive," vol. 88, no. 5, pp. 588–596, May 1969.

[28] S. D. Sudhoff and O. Wasynczuk, "Analysis and average-value modeling of line-commutated converter-synchronous machine systems," vol. 8, no. 1, pp. 92–99, Mar. 1993.

[29] S. D. Sudhoff, "Analysis and average-value modeling of line commutated converter-synchronous machine systems," vol. 8, no. 3, pp. 408–410, Sep. 1993.

[30] S. D. Sudhoff, K. A. Corzine, H. J. Hegner, and D. E. Delisle, "Transient and dynamic average-value modeling of synchronous machine fed load-commutated converters," vol. 11, no. 3, pp. 508–514, Sep. 1996.

[31] J. T. Alt, S. D. Sudhoff, and B. E. Ladd, "Analysis and average-value modeling of an inductorless synchronous machine load commutated converter system," vol. 14, no. 1, pp. 37–43, Mar. 1999.

[32] I. Jadric´, D. Borojevic‘, and M. Jadric´, "A simplified model of a variable speed synchronous generator loaded with diode rectifier," vol. 1, pp. 497–502, Jun. 1997.

[33] I. Jadric´, D. Borojevic´, and M. Jadric´, "Modeling and control of a synchronous generator with an active dc load," vol. 15, no. 2, pp. 303–311, Mar. 2000.

[34] J. Jatskevich, S. D. Pekarek, and A. Davoudi, "Parametric average-value model of synchronous machine-rectifier systems," vol. 21, no. 1, pp. 9–18, Mar. 2006.

[35] S. A. Tahan and I. Kamwa, "A two-factor saturation model for synchronous machines with multiple rotor circuits," vol. 10, no. 4, pp. 609–616, Dec. 1995.

[36] O. Wasynczuk and J. V. Jatskevich, "Circuit simulation," U.S. Patent 7 353 157, Apr. 1, 2008.

[37] S. D. Pekarek, O. Wasynczuk, and H. J. Hegner, "An efficient and accurate model for the simulation and analysis of synchronous machine/converter systems," vol. 13, no. 1, pp. 42–48, Mar. 1998.

Vita

Thaer Qunais was born in Amman, Jordan. He received his Bachelor degree in the field of Electrical and Computer Engineering from The Hashemite University, Az Zarqa, Jordan in June 2010. In August 2011, he enrolled as a MSEE student in the Department of Electrical and Computer Engineering at the University of Kentucky.